Influences of up-milling and down-milling on surface integrity and fatigue strength of X160CrMoV12 steel

Adnen Laamouri [1,2] · Farhat Ghanem [3] · Chedly Braham [4] · Habib Sidhom [3]

Abstract
This paper aims to compare the influences of the two peripheral milling modes, up-milling and down-milling, on surface integrity and fatigue strength of X160CrMoV12 high-alloy steel. The experimental investigations showed an important difference between integrity of both milled surfaces. The down-milled surface is lowly work-hardened and well finished (lower roughness), but subjected to tensile residual stresses and severely damaged by folds of metal and short micro-cracks. The up-milled surface is highly work-hardened and subjected to compressive residual stresses, but poorly finished (higher roughness) and damaged by a density of micro-cavities due to carbide extraction. The results of 3-point bending fatigue tests revealed that the fatigue limit at 2×10^6 cycles of the up-milled state is largely higher of about 26% in comparison with the down-milled state. The effects of surface integrity induced by each milling mode on fatigue strength were evaluated using a HCF behaviour predictive approach based on Dang Van's multiaxial criterion. The predictive results estimated that the pre-existing micro-cracks play a dominant role in the fatigue strength degradation of the down-milled surface while the other surface effects seem to be lower. On the contrary, the fatigue strength of the up-milled surface is less affected by the pre-existing micro-cavities. The detrimental roughness effect (stress concentration effect) is significantly reduced by the beneficial effects of superficial hardening and compressive residual stresses. So, this study revealed that up-milling is the more appropriate mode for a better surface integrity towards fatigue strength of X160CrMoV12 steel than the down-milling mode.

Keywords Up-milling · Down-milling · Surface integrity · Fatigue · Dang Van's criterion

1 Introduction

Milling is the machining process that removes material from a workpiece by combining the rotation of a multiple cutter tool and the advancing (or feeding) of the workpiece in a direction at an angle with the axis of the tool [1]. This process presents two distinct ways to cut materials namely, conventional (or up) milling and climb (or down) milling. The difference between these two techniques is the relationship of the rotation of the cutter to the direction of feed. In up-milling, the cutter rotates against the direction of the feed, while during down-milling, the cutter rotates with the feed (Fig. 1).

It is well established that the cutting forces and thermal gradients generated by the up-milling and down-milling modes during the contact tool-material are not identical [2, 3]. Consequently, the machined surface integrity (including surface roughness, micro-structural changes, residual stresses and sometimes damaging defects) is certainly different [4–6] as well as the tool wear rate [7–9] and also the dynamic stability of milling process [10].

✉ Adnen Laamouri
adnen_laamouri@yahoo.fr

[1] Unity of Mechanical Production Engineering and Materials (UGPMM, UR17ES43), National School of Engineers of Sfax (ENIS), University of Sfax, Route de Soukra km 4 BP, 1173-3038 Sfax, Tunisia

[2] Higher Institute of Applied Sciences and Technology of Sousse (ISSATSO), University of Sousse, Avenue Ibn Khaldoun, Cité Taffala, 4003 Sousse, Tunisia

[3] Laboratory of Mechanics, Materials and Processes (LMMP, LR99ES05), Higher National School of Engineers of Tunis (ENSIT), University of Tunis, 5, Avenue Taha Husseïn, Montfleury, 1008 Tunis, Tunisia

[4] Laboratory of Processes and Engineering in Mechanics and Materials (PIMM, UMR CNRS 8006), ENSAM, 151, Boulevard de l'Hôpital, 75013 Paris, France

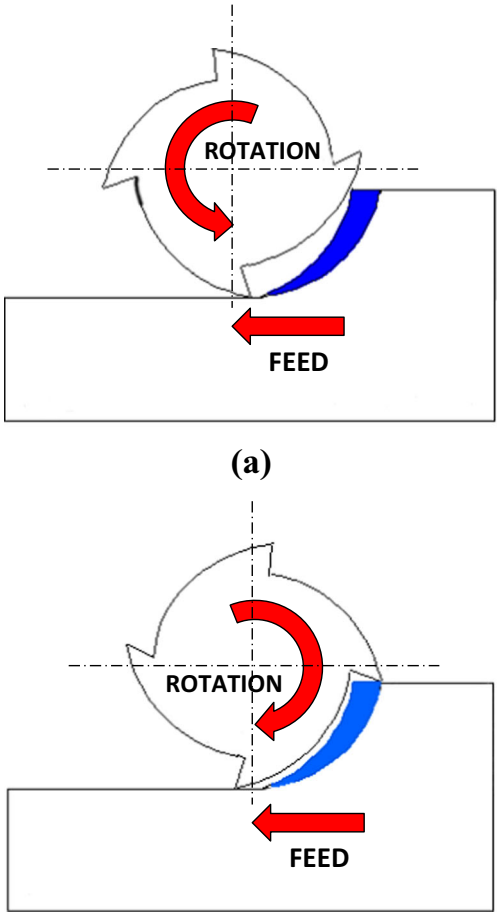

Fig. 1 The two peripheral milling modes: up-milling (**a**) and down-milling (**b**)

The temperature effect, favoured in down-cut milling, induces tensile residual stresses, while the work-hardening, favoured in up-milling, induces compressive residual stresses. Scholtes [5] showed, for a recrystallized 0.45% steel, that the residual stress distribution in longitudinal and transverse directions to the grooves after up-milling is compressive, while it is tensile after down-milling. The up-milling stresses are higher in the transverse direction, but the down-milling stresses are higher in the longitudinal direction. If the workpiece is made of hardenable steel, martensite may form due to the rapid heating and cooling, causing compressive residual stresses.

Surface roughness is generally higher for the down-milled surfaces in comparison with the up-milled ones. A recent work [11] deals with thin-walled components from steel C45 machined by the two milling processes revealing that the values of the surface roughness (Rz) for the up-milled surface are almost two times higher and present more fluctuations than for the down-milled surface. This difference was explained by several factors such as rigidity of ribs, type of machining and forces corresponding to the type of milling.

It is well known that the machining surface integrity influences strongly the fatigue lifetime of materials, since fatigue micro-cracks initiate always at the surface [12–17]. For this reason, several studies have been dedicated to the effects of milling on fatigue behaviour of many materials, particularly aluminium and titanium alloys, and superalloys widely used to manufacture structural parts for aviation and aerospace industries [18–25]. It was proved that residual stresses and surface roughness, particularly, could affect considerably the performance of the milled materials under high cyclic fatigue (HCF) load.

Residual stress can play a crucial factor towards fatigue performance of milled parts. Compressive residual stress is usually advantageous to the fatigue life of machined parts, while residual tensile stress is the opposite. The tensile residual stress promotes the nucleation and extension of fatigue micro-cracks. When the crack increases to a certain extent, it will cause workpiece failure [26]. So, it is necessary to ovoid tensile residual stresses occurring during the machining process. However, when the cyclic loading produces plastic deformation, the effect of residual stress will be reduced or disappeared [15, 27]. In view of the high-speed milling process of Ti-10V-2Fe-3Al, Yao et al. [28] found that the fatigue life of the workpiece is more sensitive to residual stress than to surface roughness. The influence of the milling process on the fatigue life of Ti6-Al-4V was investigated by Moussaoui et al. [29]. They found that residual stress has a more preponderant influence on fatigue life than the geometric and metallurgical parameters. Huang et al. [30] studied the effect of different tool paths on the fatigue life of AISI H13 high-speed milling process. The results show that the different tool paths lead to the difference in effective residual stress, which results in different fatigue performance of the workpiece. Meanwhile, it is found that the influence of effective residual stress on the fatigue life of the workpiece is greater than that of the orientational surface topography. Yang et al. [31] studied the effect of residual stress on the fatigue life of workpieces during milling of Ti-6Al-4V. The results show that increasing the compressive residual stress can effectively improve the fatigue performance of the workpiece.

Surface roughness, considered one of the main properties of machined surface integrity, can strongly reduce fatigue performance of a mechanical workpiece [14]. Generally, it is expected to encourage fatigue crack initiation due to microscopic stress concentration induced by pits and grooves, particularly, for hard materials. Many researchers investigated the effect of milling surface roughness on fatigue life of materials. The semi-empirical model of the stress concentration factor (K_t), proposed by Arola et al. [32, 33] and based on standard roughness parameters (*Ra*, *Ry* and *Rz*), was used. Wang et al. [34] found that high surface roughness leads to a high-stress concentration coefficient, which reduces the fatigue life of the workpiece. Yao et al. [35] presented the effects of high-speed down-milling parameters on the surface topography and

fatigue behaviour of a titanium alloy. The results have shown that predicting the fatigue life of specimens based on the surface stress concentration factor, proposed by Arola et al., is more accurate than that based on the Ra surface roughness parameter. Novovic et al. [36] investigated the effect of surface and subsurface condition on the fatigue life of Ti alloy workpiece. Their research results indicated that the surface topography, in particular texture direction, has a strong correlation with the fatigue life of workpiece. Huang et al. [30] studied the effect of different tool paths on the fatigue life of AISI H13 high-speed milling process. It was noted that different tool paths lead a the difference in microscopic stress concentration caused by the orientation morphology, which affects the fatigue performance of the workpiece. Liu et al. [37] showed that modified fatigue life of Incoloy A286 alloy (iron-based superalloy) under different face milling parameters was mainly determined by the roughness and mechanical properties, including the yield strength and fracture toughness, rather than the residual stresses, because of a severe stress relaxation. Yang et al. [38] investigated the effect of surface topography induced by peripheral down-milling on low cycle fatigue performance of titanium alloy Ti-6AL-4V. They showed that the fatigue life model based on surface stress concentration factor that calculated using three-dimensional surface roughness parameters is more accurate than that using two-dimensional ones.

This review of the literature revealed the existence of some works which deal with the comparison of up- and down-milling configurations in terms of residual stress and surface roughness. Generally, these two effects were found contradictory for up-milling (compressive stresses and higher roughness) and present respectively opposite effects (tensile stresses and lower roughness) for down-milling. However, there is no works related to the different effects on surface integrity, including mechanical, micro-structural, micro-geometrical and damaging effects. In addition, their respective contributions on HCF behaviour of material are not well known. The lack of some works in this context represents a great difficulty to control and optimize the parameters of milling process for a better performance of materials.

This work presents an experimental and predictive study to compare both up-milling and down-milling modes in terms of surface integrity (stabilized residual stresses, work-hardening, roughness and damaging defects) and fatigue behaviour of an annealed EN X160CrMoV12 steel. The respective fatigue limits were determined at 2×10^6 cycles under 3-point bending tests ($R_\sigma = 0.1$). Initial and stabilized residual stresses were analysed by the X-ray diffraction method. The role of surface integrity on nucleation and growth of fatigue micro-cracks was analysed by SEM observations. The evaluation of surface integrity effects on fatigue strength was carried out using a predictive approach [39] based on Dang Van's multiaxial fatigue criterion [40].

2 Material and experimental procedure

2.1 Material

The material used in this study is an EN X160CrMoV12 high-alloy steel, essentially used in the manufacturing of tools and moulds by using the milling process. The micro-structure of this steel at the annealed state is composed of ferritic matrix with a dense distribution of spheroidal and elongated carbide grains, essentially of chrome, with different sizes which do not exceed 30 μm (Fig. 2). Its chemical composition is recapitulated in Table 1, and its principal mechanical characteristics, given in Table 2, were determined by tensile test on normalized specimens, carried out using a tensile test machine type MTS.

2.2 Machining conditions

The influence of up-milling and down-milling, respectively, on surface integrity and fatigue behaviour of X160CrMoV12 steel was studied by application of each milling mode (Fig. 3) to two sets of V-notched fatigue specimens ($Kt = 1.6$) using a CNC milling centre. The table of this machine was equipped with a device type Kistler composed of three dynamometers for measuring cutting forces. The machining conditions used in this study are reported in Table 3.

2.3 Surface characterization

The superficial hardening due to each milling operation was characterized by Vickers micro-hardness filiation under a load of 0.05 Kg, in-depth of the specimen notch root. The in-depth residual stress distributions were analysed by the X-ray diffraction (XRD) technique using a diffractometer with the conditions indicated in Table 4. The two-dimensional roughness profiles of both up-milled and down-milled surfaces were measured by a stylus instrument and characterized by two

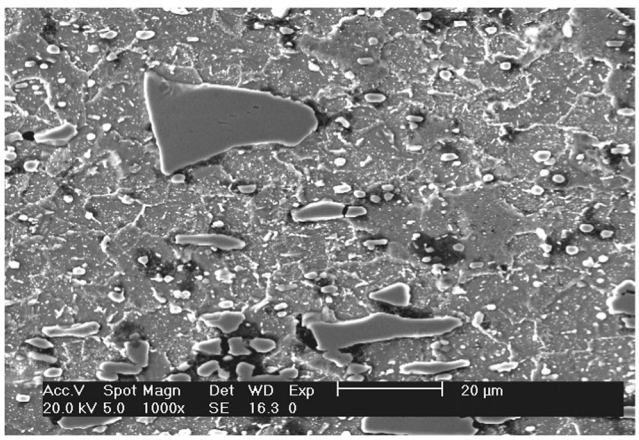

Fig. 2 Micro-structure of an annealed EN X160CrMoV12 steel

Table 1 Chemical composition of the EN X160CrMoV12 steel

C	Si	Mn	P	S	Cr	Mo	V	W	Fe
1.58	0.26	0.32	0.01	0.01	12.03	0.16	0.4	0.01	Balance

standard parameters according to the standard ISO of geometrical product specifications (GPS) [41]: the arithmetical average roughness (Ra) and the maximum roughness depth (R_{max}). The surface defects have been examined and characterized by SEM observations at the notch root of specimens.

2.4 Fatigue tests

The influences of up-milling and down-milling on HCF behaviour have been evaluated by 3-point plane bending fatigue tests on the two sets of V-notched specimens machined by the two milling modes (Fig. 4). These tests have been performed using a MTS machine with a stress ratio $R_\sigma = \sigma_{min}/\sigma_{max} = 0.1$ and a frequency of 15 Hz. The staircase method has been used to determine the corresponding fatigue limits at 2×10^6 cycles and 50% failure probability. The influence of surface integrity on stages of nucleation and growth of fatigue micro-cracks has been studied by SEM observations at the notch root of fractured specimens. The stabilized residual stress profiles near fatigue limit of each milled state were measured in no-fractured specimens and compared with the initial profiles.

3 Results

3.1 Surface properties

The parameters of surface integrity for both milling modes and their effects on fatigue limit of the EN-X160CrMoV12 steel are summarized in Table 5. These parameters seem to be depending on thermic fields and cutting forces for each milling mode. The cutting forces in longitudinal and transverse directions (F_x and F_z) appear obviously greater in the case of up-milling owing to the important friction effect of teeth of the cutting tool on the machined surface (Fig. 5). For both milling modes, the

Table 2 Tensile properties of the EN X160CrMoV12 steel

Young modulus, E (MPa)	207,000
Poisson's ratio, ν	0.3
0.2% offset yield stress, σ_y (MPa)	595
Ultimate stress, σ_u (MPa)	733
Fracture stress, σ_f (MPa)	681
Elongation, A (%)	20
Material constant of the Hollomon relationship, K (MPa)	968
Strain-hardening coefficient, n	0.119

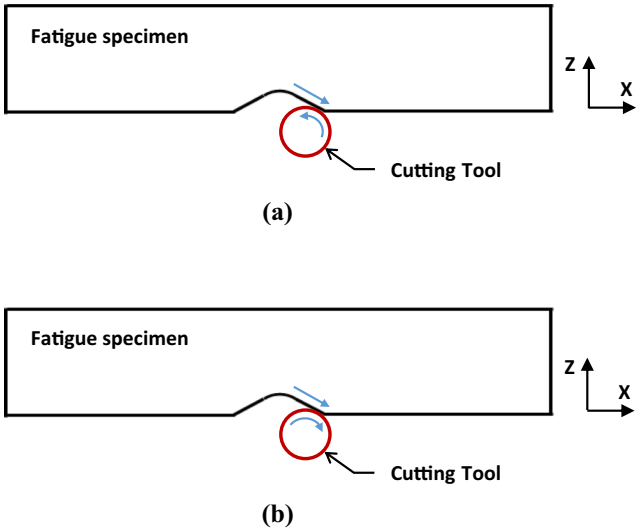

Fig. 3 Application of the two milling modes for machining of the notch of fatigue specimens: up-milling (**a**) and down-milling (**b**)

cutting force in the vertical direction (F_y) is nearly insignificant, but the more important forces were recorded into the principal penetration direction of the cutting tool in the material (F_x for the up-milling and F_z for the down-milling). The temperature fields have not been recorded, but the metallographic observations of the cross-sections of the machined samples by up-milling (Fig. 6a) and down-milling (Fig. 6b) revealed the absence of any metallurgical transformations at the near-surface layers. These observations confirm that the temperatures reached at these layers are still lower than the metallurgical transformation temperature of the studied steel (< 700 °C).

3.1.1 Surface roughness

Figure 7 a and b depict, respectively, the roughness profiles of up-milled and down-milled surfaces recorded along 5 mm. They reveal that the up-milling operation involves a greater micro-geometrical state of machined surface than the down-milling operation. In fact, Ra value is two times higher for the up-milled surface, and furthermore, the R_{max} parameter is more significant for this surface, and three times greater (Table 5).

Table 3 Machining parameters

Milling mode	Up-milling/down-milling
Feed rate, f_z (mm/tr.tooth)	0.1
Cutting speed, v (m/min)	20
Cutting depth, a_p (mm)	0.2
Lubrication	Soluble oil
Cutting tool	Material (HSS), ∅ = 6 mm, Z = 4

Table 4 XRD conditions

Target	Cr
Wavelength $K_{\alpha 1}$, Å	2.2897
Filter	V
Diffraction plane hkl	211
Bragg angle (°)	156.3
Current (mA)	5
Voltage (kV)	20
Goniometer tilt	Psi
Beam section ∅ (mm)	1.5
Young's modulus for steel, E (GPa)	210
Poisson's ratio, ν	0.33
Number of ψ angles	13, from − 36.3° to + 39.2°
Number of ϕ angles	2, 0° and 90°

3.1.2 Damage defects

In the case of up-milling, an excessive crashing of matter with a density of micro-cavities most likely associated with the extraction of chrome-carbides was revealed (Fig. 8a, b). In the case of down-milling, the SEM observations of machined surface (Fig. 9a, b) reveal an important density of defects (micro-cracks and matter folds).

3.1.3 Superficial work-hardening

The micro-hardness profiles (HV) measured in-depth of up-milled and down-milled surfaces are given in Fig. 10. The up-milled surface is characterized by an important superficial hardening with a surface maximum value $HV_s/HV_0 = 175\%$ and a hardened layer of 300-μm thickness. On the contrary, the superficial hardening is lower ($HV_s/HV_0 = 145\%$) and limited to 50 μm in the case of down-milled surface.

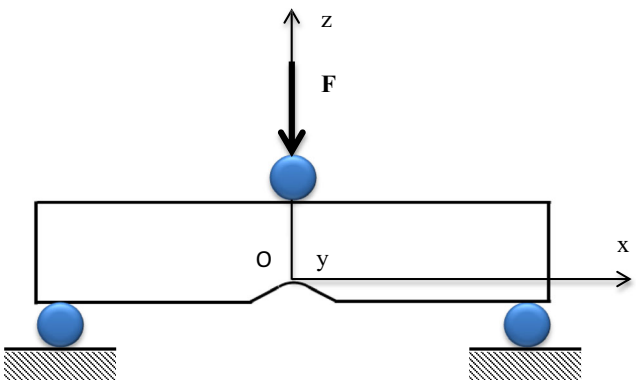

Fig. 4 The 3-point plane bending fatigue test applied to a V-notch specimen ($Kt = 1.6$)

3.1.4 Initial residual stresses

For the up-milled surface, the in-depth residual stress profiles in both longitudinal and transversal directions of sample (Fig. 11) are compressive until a depth of approximately 300 μm and remain low in the bulk (≈ − 50 MPa). The maximum values are reached at the surface with the following values: $\sigma_{Rxx} \approx -300$ MPa and $\sigma_{Ryy} \approx -180$ MPa, in the longitudinal and transversal directions, respectively.

For the down-milled surface, the initial residual stresses are lower, with surface tensile value in the longitudinal direction and compressive value in the transversal direction. These stresses are maximal at the surface ($\sigma_{Rxx} \approx -50$ MPa; $\sigma_{Ryy} \approx +100$ MPa) and decrease rapidly to remain tensile stresses of ≈ + 50 MPa at a depth nearly equals to 100 μm.

3.2 HCF behaviour

The results of fatigue tests, reported on the SN diagram (Fig. 12), show that for the same loading level, the fatigue life is higher for the up-milled state. The application of the staircase method for the experimental results gives a fatigue limit at 2×10^6 cycles of the up-milled surface significantly higher than that of the down-milling (Table 5). This improvement of HCF behaviour, of about 26%, in comparison with the down-milled state can be explained by the influence of surface integrity which appears beneficial for fatigue strength of the up-milled sample.

The SEM exams of the notched root of fractured and non-fractured samples by fatigue permitted to clarify the role of specific defects for each milling mode on nucleation and propagation of fatigue micro-cracks. For the down-milled surface, it seems difficult to define the nucleation stage since these surfaces present already a distribution of short micro-cracks (of 2 to 10 μm) linked to folds and associated with matter removing mode (Fig. 9). Under the effect of cyclic loadings, these micro-cracks and especially of overlays, grow at the surface (Fig. 13) and subsurface, and then they coalesce into forming a network of long cracks which are responsible for fatigue fracture. The exams of the machined surface by up-milling reveal fatigue micro-crack nucleation associated with multiple carbide/ferrite detachments and carbides extraction (Fig. 14). These micro-cracks are linked after growth under cyclic loading and become long cracks which are responsible for final fracture by fatigue.

For both up-milled and down-milled surfaces, initial residual stresses relax under fatigue loading and reach a stabilized state after 2×10^6 cycles at fatigue limit (Fig. 15). Initial residual stresses, principally tensile stresses, acting in the down-milled surface, were transformed into compressive stresses in the superficial layers (Fig. 15a). Their stabilized values at the surface are compressive, particularly in the transversal direction ($\sigma^*_{Rxx} = -150$ MPa; $\sigma^*_{Ryy} = -30$ MPa). On the other hand, the

Table 5 Influence of milling mode on cutting forces, surface integrity and HCF behaviour of EN X160CrMoV12 steel

Milling mode	Cutting forces (daN)			Surface integrity						HCF behaviour	
				Roughness (μm)		Residual stresses (MPa)		Surface defects	Work-hardening HV_s/HV_0 (%)	Endurance limit at 2×10^6 cycles, σ_e (MPa)*	Difference (%)**
	F_x	F_y	F_z	R_a	R_{max}	σ_{Rxx}	σ_{Ryy}				
Up-milling	70	0	45	11	87	− 300	− 180	Crashing of matter, micro-cavities	175	430 ± 12	26%
Down-milling	25	0	40	5	28	− 50	+ 100	Folds, micro-cracks	145	340 ± 15	–

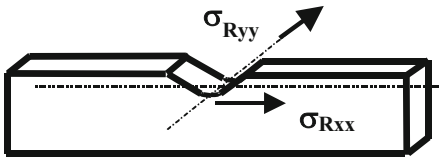

*σ_e is expressed in terms of maximal stress

**The endurance limit of the down-milled sate is taken as reference

compressive residual stresses acting in the up-milled surface relax partially (Fig. 15b) and remain compressive stresses at the surface ($\sigma^*_{Rxx} = -150$ MPa;$\sigma^*_{Ryy} = -75$ MPa).

4 Predictive evaluation

4.1 Dang Van's criterion

The effects of both up-milling and down-milling on fatigue strength were evaluated using the HCF behaviour predictive approach developed in previous work [39]. This approach is based on Dang Van's multiaxial criterion [40] in which the surface integrity parameters including residual stresses, work-hardening, surface roughness and damage defects are taken into account. For the sake of simplicity, Dang Van's criterion has been applied at milled surfaces of the sample notch root where the fatigue cracks occurred. This criterion is expressed,

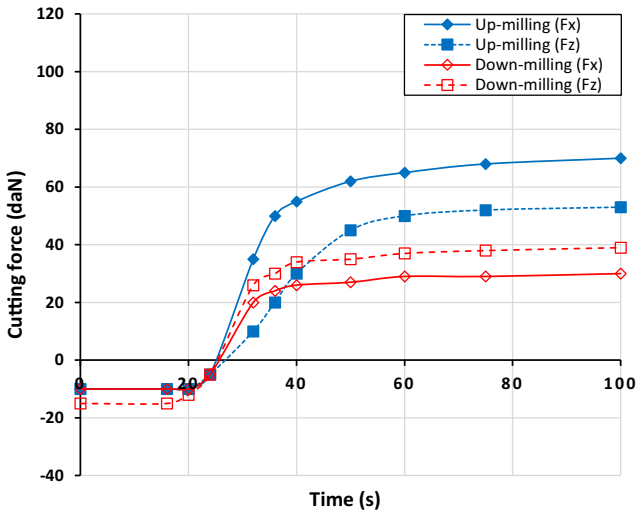

Fig. 5 Evolution of cutting forces with time under the two milling modes

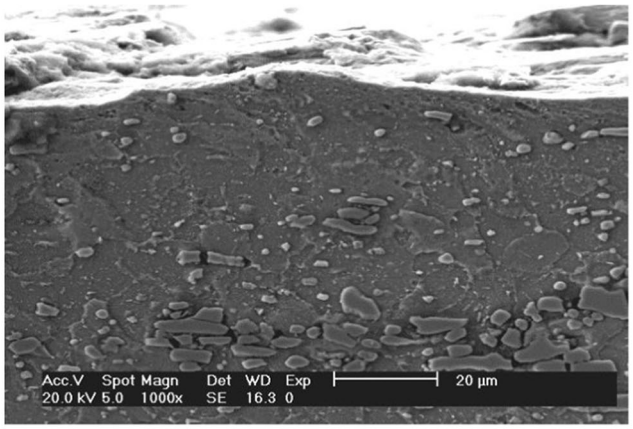

(a)

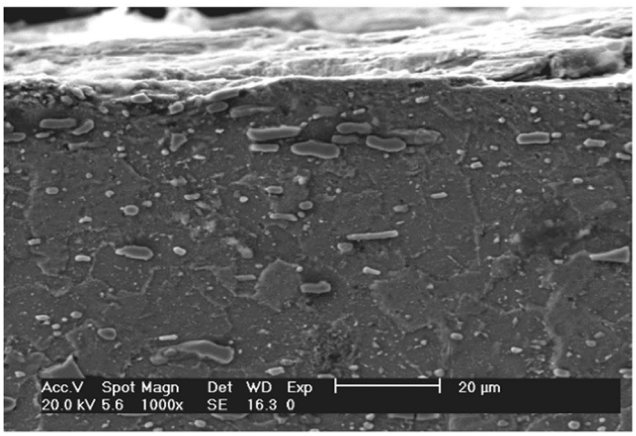

(b)

Fig. 6 Cross-section SEM micrographs of the up-milled sample (**a**) and the down-milled sample (**b**)

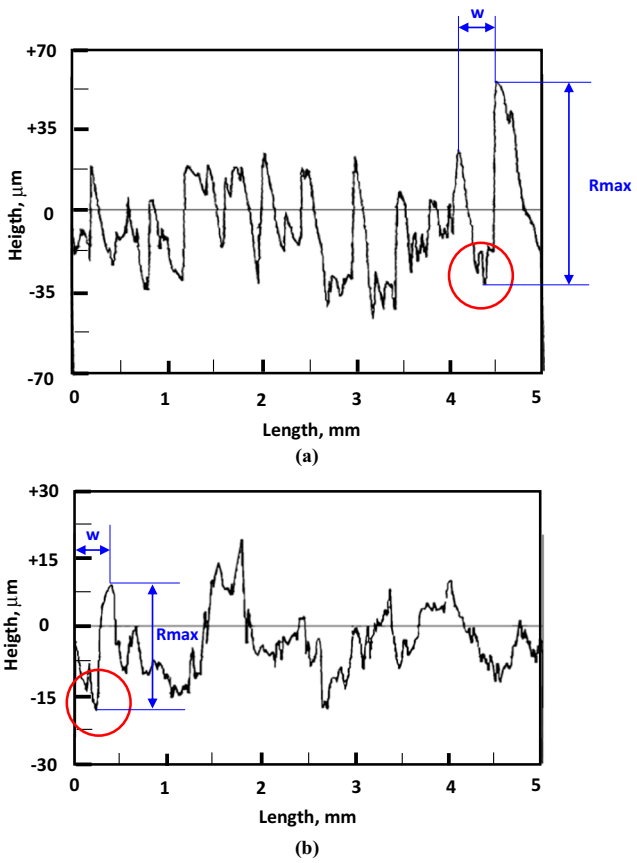

Fig. 7 Roughness profiles: up-milled surface (**a**) and down-milled surface (**b**)

in the case of proportional loadings, by the limitation of equivalent stress (σ^{eq}) given by a linear relationship of two parameters (τ^a and $P^{\max}$) of the cyclic stress tensor (Eq. 1).

$$\sigma^{eq} \equiv \tau^a + \alpha_0 . P^{\max} \leq \beta_0 \quad (1)$$

where τ^a and $P^{\max}$ are, respectively, Tresca's stress amplitude and the maximum hydrostatic pressure.

The α_0 and β_0 constants define the multiaxial fatigue threshold of the base material. They were identified by using two uniaxial fatigue tests: a fully reversed torsion limit (t_{-1}) and a fully reversed bending limit (f_{-1}) on smooth specimens, according to empirical relationships for steels [42]. Consequently, the base material constants α_0 and β_0 are equal to 0.3 and 201 MPa, respectively.

4.2 Prediction of the roughness effect

The value of maximum roughness depth of the up-milled surface ($R_{\max}$ = 87 µm) and that of the down-milled one ($R_{\max}$ = 28 µm) indicates that the surface roughness can have an important influence on fatigue strength of both milled states [14, 43]. The two-dimensional roughness profiles (Fig. 7) depict that both milled surfaces are characterized by irregular micro-

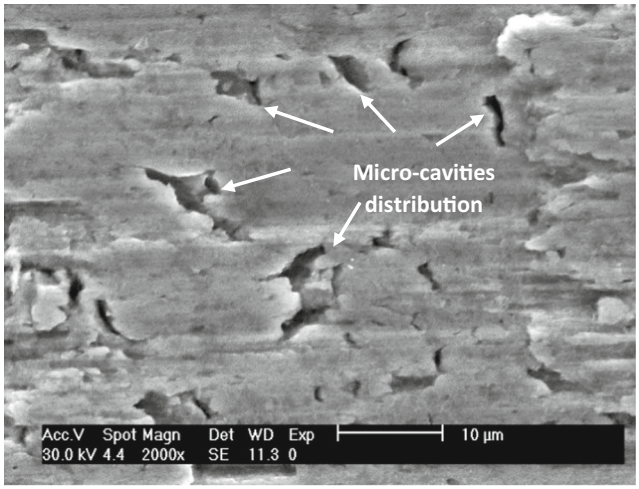

(a)

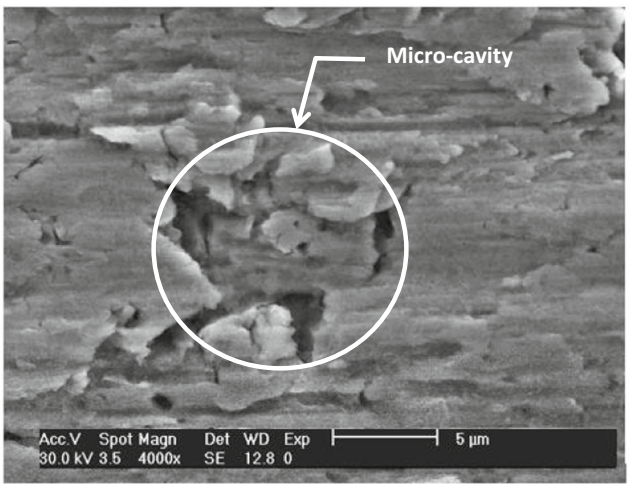

(b)

Fig. 8 SEM micrographs showing a micro-cavity distribution at the up-milled surface: magnification× 2000 (**a**) and magnification × 4000 (**b**)

asperities in the form of blunt micro-notches. For this reason, the milling roughness effect can be considered as a stress concentration effect induced by the deepest and sharpest grooves, and not as a micro-crack effect [43]. The milling roughness effect can then be described through the fatigue stress concentration factor $(\hat{K}_f)$. This factor is defined as the ratio between the fatigue limit of an un-notched (smooth) specimen and the fatigue limit of a notched (rough) specimen, and it can be related to the stress concentration factor $(\hat{K}_t)$ [43]. Ås et al. [44, 45] proposed to calculate $\hat{K}_t$ from FE simulations of the surface topography. The application of this method to a 6082.52-T6 aluminium alloy prepared with emery paper provided more accurate fatigue life prediction than the semi-empirical model proposed by Arola et al. [32, 33], since the stress concentration estimation is based upon local measurements rather than averaged geometrical parameters.

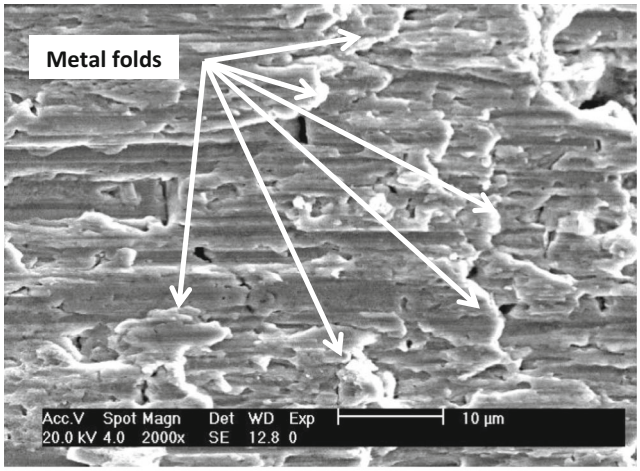

(a)

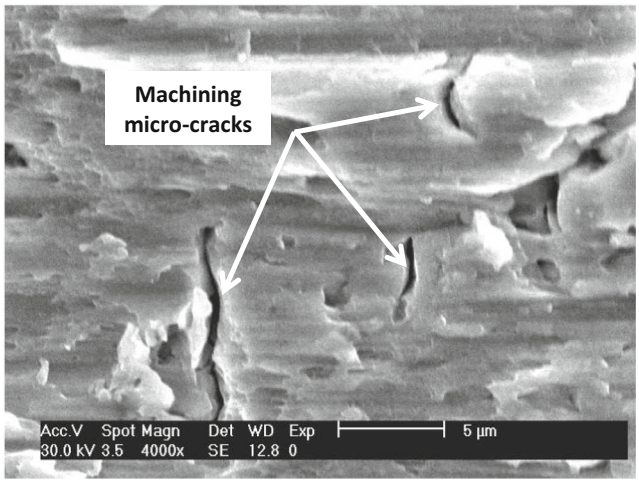

(b)

Fig. 9 SEM micrographs showing a distribution of folds and micro-cracks in the down-milled surface: magnification× 2000 (**a**) and magnification × 4000 (**b**)

In this work, the potential site of fatigue failure (with the highest stress concentration effect due to a micro-geometrical defect) is identified by the R_{max} roughness parameter (Fig. 7). For the sake of simplicity, this potential site is modelled by using a critical micro-notch in semi-circular shape localized at the sample notch root and characterized by a height h (equals to R_{max}) and a width w (equals to the distance between the two peaks of the critical defect). For both milled surfaces, w is approximately equal to 700 µm.

The stress micro-concentration effect due to the presence of this critical micro-notch in the notch root of milled samples was evaluated by using the finite element (FE) method. For each case (non-milled sample, up-milled sample and down-milled sample), a 3D elastic FE model was developed using the commercial FE software ABAQUS/standard [46]. Due to symmetry conditions, only one-quarter of the 3-point bending test was modelled (Fig. 16). The following boundary conditions were applied to the FE models: (i) An X-symmetry

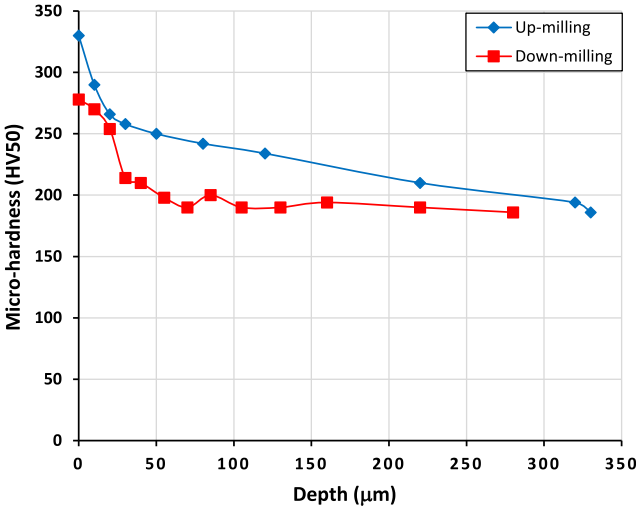

Fig. 10 In-depth micro-hardness profiles

condition (Ux = URy = URz = 0) is applied to the cross-section at the half-length; (ii) a Y-symmetry condition (Uy = URx = URz = 0) is applied to the surface at the half-thickness; (iii) a fixed roller, considered as an analytical rigid part, is placed in perfect contact near the extremity of the quarter sample and (iv) a mobile roller is placed in perfect contact with the sample at the central plane and on the opposite side to the notch (Fig. 16a). This roller is mobile in Z-direction and subjected to a concentrated force (*F/4*) corresponding to the fatigue limit of the up-milled or down-milled sample.

A local partition of the notched zone (2 × 2.5 × 2 mm) was created and meshed using FE elements of type 8-node linear brick with reduced integration (C3D8R) with a highly refined size around the micro-notch of ≈ 0.05 × 0.05 × 0.05 mm (Fig. 16b, c). The zone outside notch was meshed using FE elements of type 4-node linear tetrahedron (C3D4) with progressively greater sizes far from the notch zone until a size of 1.5 ×

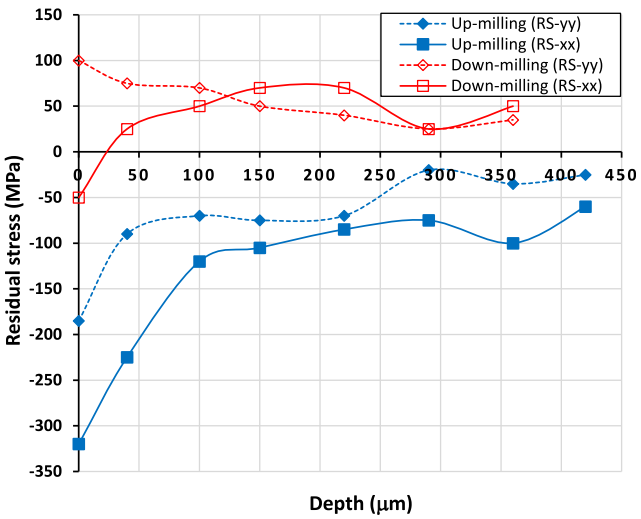

Fig. 11 Distribution of initial residual stresses in up-milled and down-milled surfaces

1.5 × 1.5 mm (Fig. 16a). The material behaviour, assigned to the sample geometry, is assumed isotropic and linear elastic with Young's modulus of 207 GPa and a Poisson's ratio of 0.3.

The results of FE simulation, presented in Figs. 17 and 18, permits to compare the distributions of normal stresses (σ_{xx},σ_{yy} and σ_{zz}) in the notch root of the non-milled surface (without micro-notch effect) and the up-milled surface (with micro-notch effect), respectively. Figure 17 shows, for the non-milled surface, a concentration of σ_{xx} and σ_{yy} stresses induced in a large zone of the sample notch root. The vertical stress σ_{zz} (normal to the notch root surface) is nearly equal to zero like the different shear stresses. The higher concentration zone is situated at the centre of the notch root where the longitudinal and transverse stresses are maximal (σ_{xx}^{max} = 670 MPa; σ_{yy}^{max} = 135 MPa). Figure 18 shows, for the up-milled surface, a very localized stress concentration zone in the micro-notch root. This stress concentration is maximal ($\hat{\sigma}_{xx}^{max}$ = 927 MPa; $\hat{\sigma}_{yy}^{max}$ = 172 MPa) at the centre of the notch root like the non-milled surface case. The concentration effect due to the critical micro-notch is more important for the principal stress (σ_{xx}) acting in the longitudinal direction than that for the secondary stress (σ_{yy}) acting in the transverse direction. The same observations were made for the down-milled surface but the stress concentration effect due to the corresponding micro-notch is lower as explained below.

Figure 19 a and b show the calculated principal stress profiles (σ_{xx}) obtained with and without the micro-notch effect for both up-milled and down-milled states, respectively. The corresponding stress concentration factor ($\hat{K}_t^{xx}$) was determined. It is equal to 1.39 for the case of up-milling and 1.16 for the case of down-milling. The affected layer is respectively equal to 300 μm and 200 μm. By using Peterson's model [47] (Eq. 2), the fatigue stress concentration factor $\hat{K}_f^{xx}$ was estimated to 1.31 and 1.14 for up-milled and down-milled surfaces, respectively.

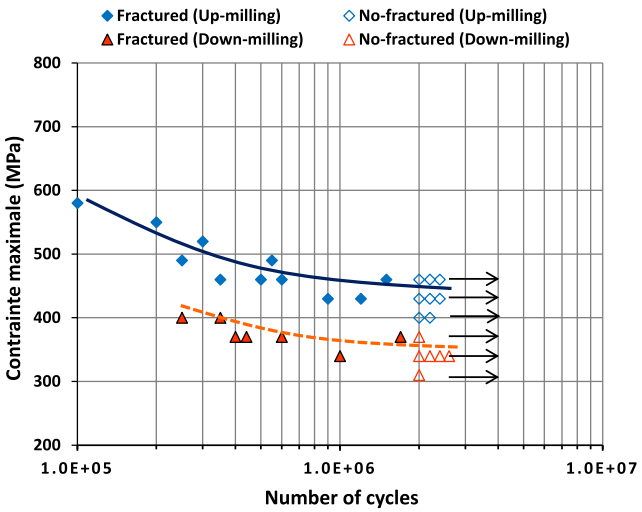

Fig. 12 Influence of milling mode on fatigue life of EN X160CrMoV12 steel (S-N diagram)

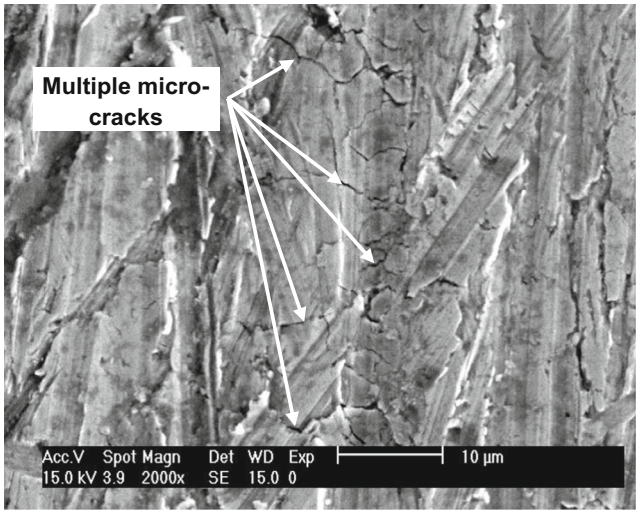

Fig. 13 Fatigue growth of pre-existing micro-cracks at the down-milled surface

$$\hat{K}_f = 1 + q\left(\hat{K}_t - 1\right) \tag{2}$$

The notch sensitivity (q) depends on the material and asperities geometry. It can be defined in terms of the effective profile valley radius of the critical defect of surface texture (ρ).

$$q = 1/(1 + \gamma/\rho) \tag{3}$$

where γ (in mm) is a material constant related to the ultimate strength (σ_u) of steels [48].

$$\gamma = 0.0254(2070/\sigma_u)^{1.8}, (\sigma_u \geq 550\ MPa) \tag{4}$$

Therefore, the micro-geometrical cyclic stress tensor $\hat{\sigma}(t)$ taking into account the critical micro-notch effect (roughness

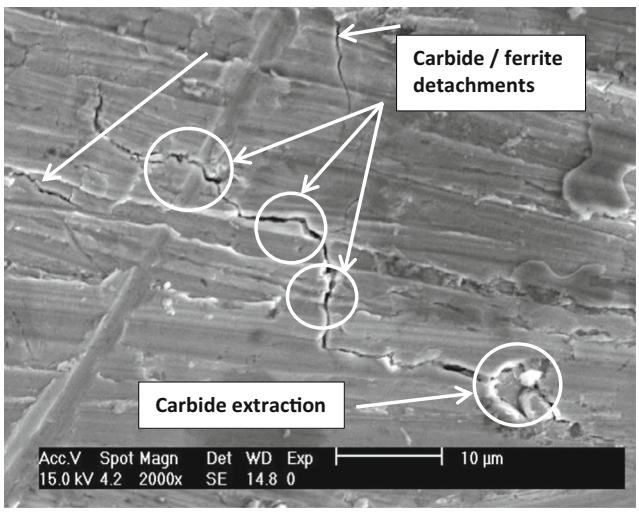

Fig. 14 Fatigue micro-crack nucleation associated with multiple carbide/ferrite detachments and carbide extraction at the up-milled surface

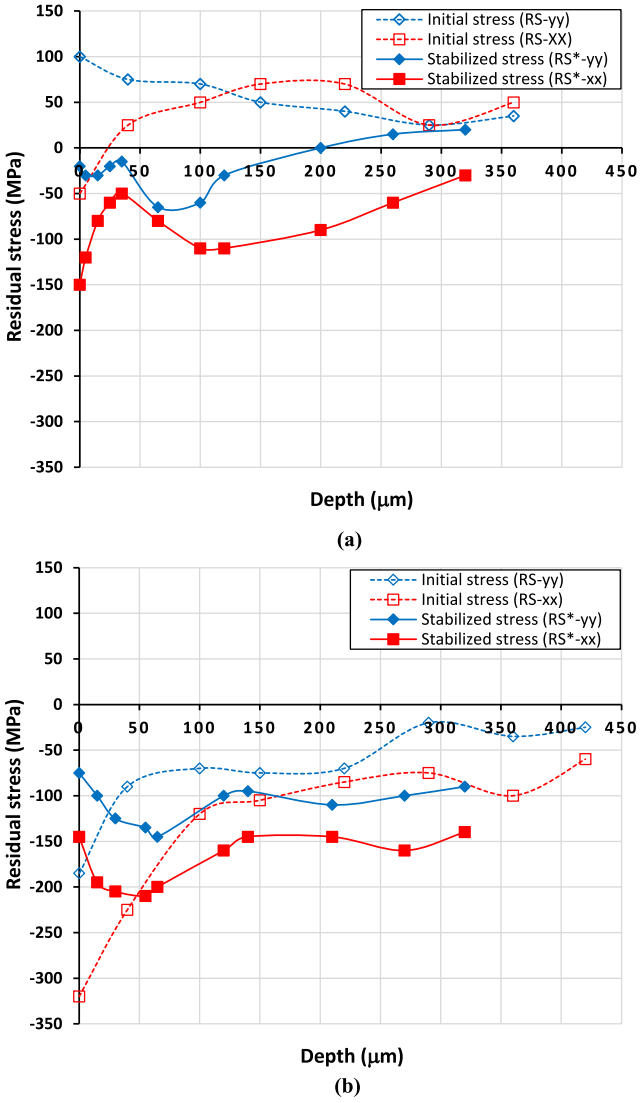

Fig. 15 Initial and stabilized residual stresses. In down-milled surface (**a**) and in up-milled surface (**b**)

effect) is biaxial (Eq. 5). The corresponding equivalent stress is deduced and given by Eq. 6:

$$\underline{\underline{\hat{\sigma}}}(t) = \begin{bmatrix} \hat{K}_f^{xx}.\left(\sigma_{xx}^a \sin(wt) + \sigma_{xx}^m\right) & 0 & 0 \\ 0 & \sigma_{yy}^a \sin(wt) + \sigma_{yy}^m & 0 \\ 0 & 0 & 0 \end{bmatrix} \tag{5}$$

$$\hat{\sigma}^{eq} = \hat{\tau}^a + \alpha_0 \hat{P}^{\max} \tag{6}$$

Where $\hat{\tau}^a = \left(\hat{K}_f^{xx}.\sigma_{xx}^a\right)/2$ and $\hat{P}^{\max} = \left(\hat{K}_f^{xx}.\sigma_{xx}^{\max} + \sigma_{yy}^{\max}\right)/3$.

The effect of roughness on fatigue strength is estimated by the indicator I_{rough} expressed by the difference between $\sigma_{\text{app}}^{\text{eq}}$ and $\hat{\sigma}^{eq}$ with respect to base material constant β_0 (Eq. 7). It is traduced in Dang Van's diagram (Fig. 20a) by a displacement of the applied loading representative point towards the failure zone. So, this detrimental effect is significantly higher for the up-milled surface ($I_{\text{rough}} \approx -20\%$), but enough low for the down-milled one ($I_{\text{rough}} \approx -6\%$).

$$I_{\text{rough}} = \frac{\sigma_{\text{app}}^{\text{eq}} - \hat{\sigma}^{eq}}{\beta_0} \tag{7}$$

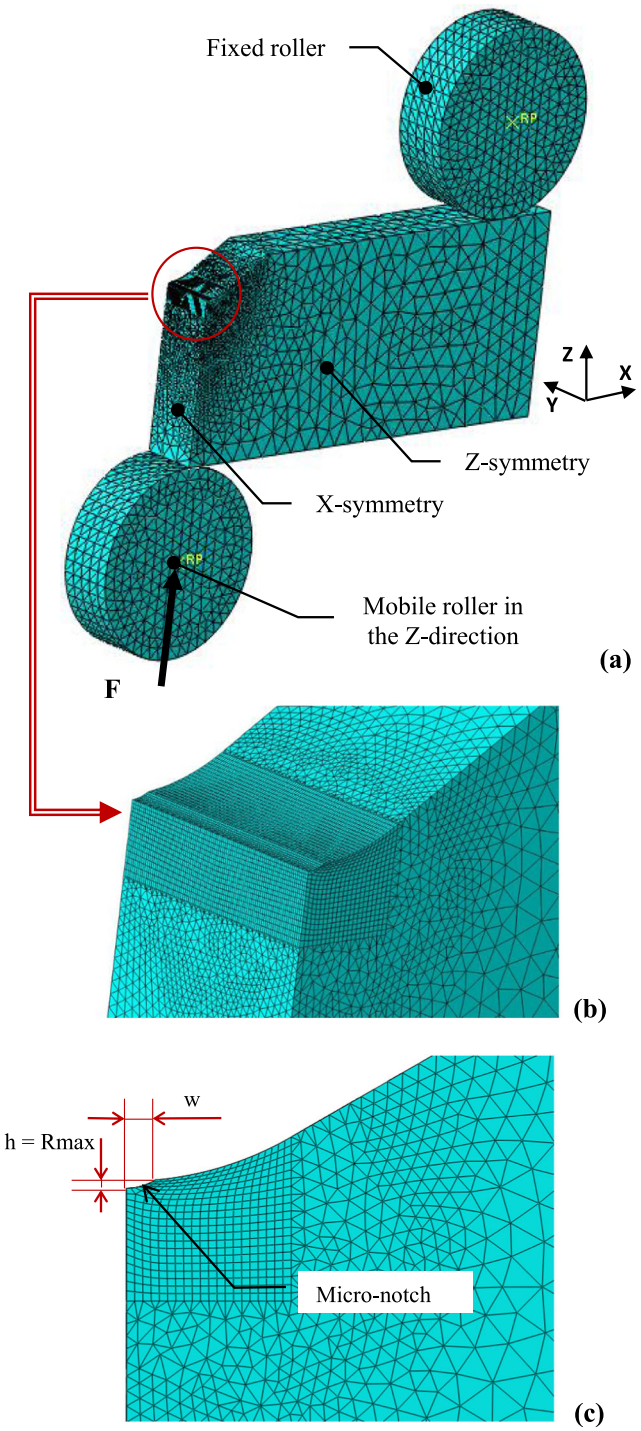

Fig. 16 **a–c** 3D elastic FE model of the 3-point test with refined meshing around the critical micro-notch at the sample notch root

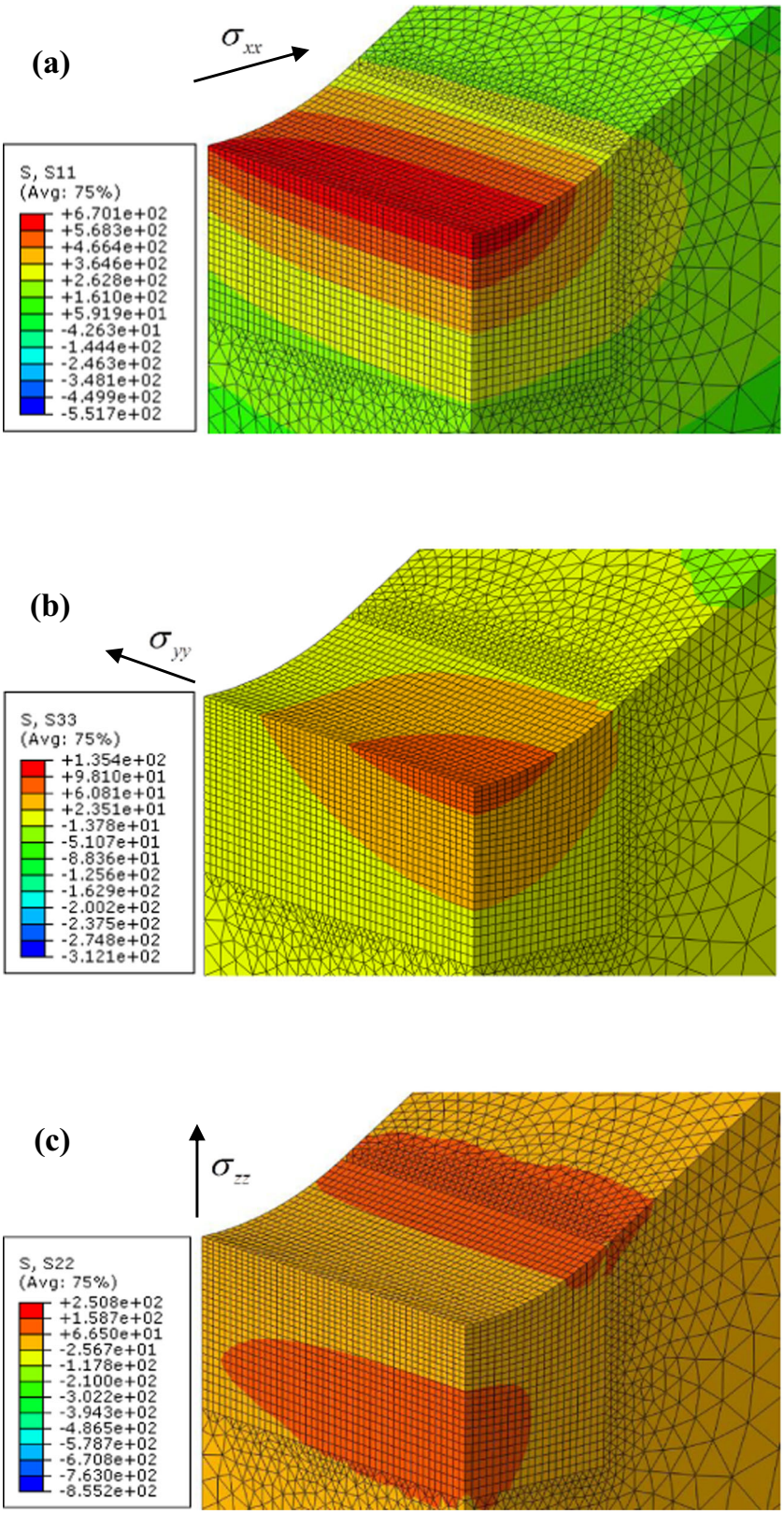

Fig. 17 Distribution of normal stresses in the sample notch root (without the presence of a micro-notch): in the x-direction (σ_{xx}) (**a**), in the y-direction (σ_{yy}) (**b**) and in the z-direction (σ_{zz}) (**c**)

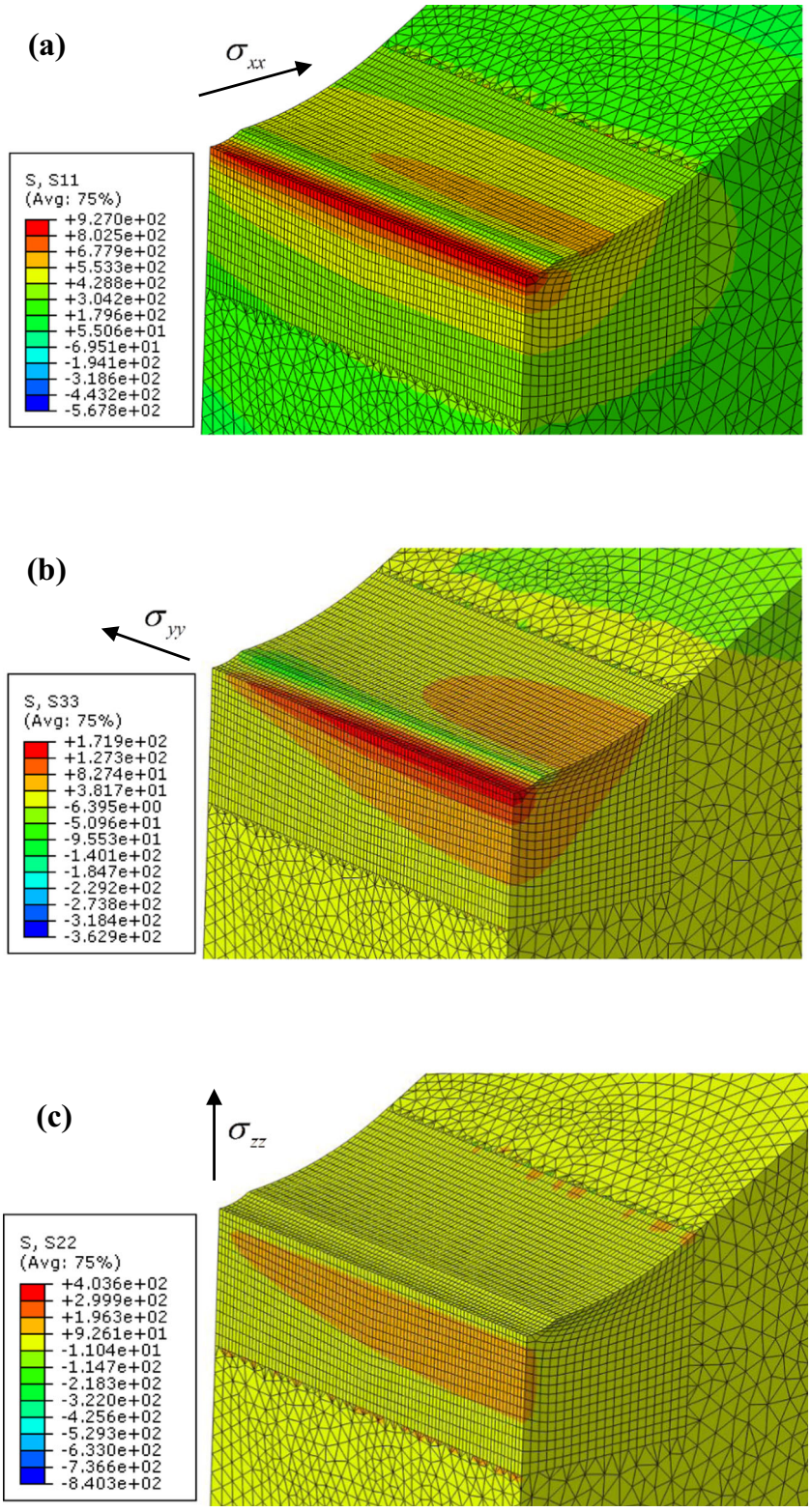

Fig. 18 Distribution of normal stresses in the sample notch root (with the presence of a micro-notch): (a) in the x-direction (σ_{xx}), (b) in the y-direction (σ_{yy}), (c) in the z-direction (σ_{zz})

4.3 Prediction of the residual stress effect

The surface residual stresses generated by the two milling conditions change and reach stabilized states under cyclic loadings corresponding to fatigue limits (Eq. 8). These stresses are compressive and beneficial for fatigue strength. So, the effective cyclic stresses acting at the potential crack nucleation site (notch root) should be evaluated by taking into account

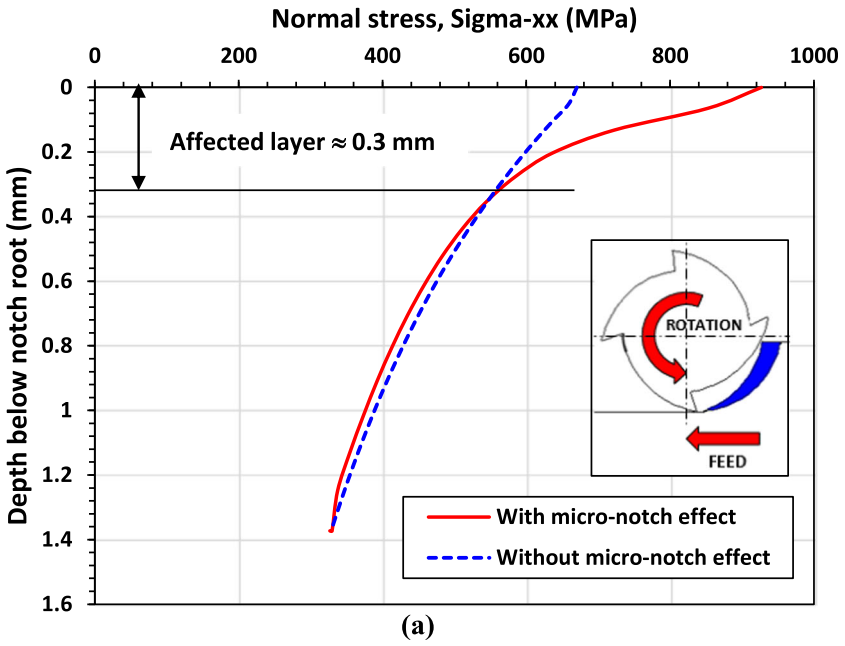

(a)

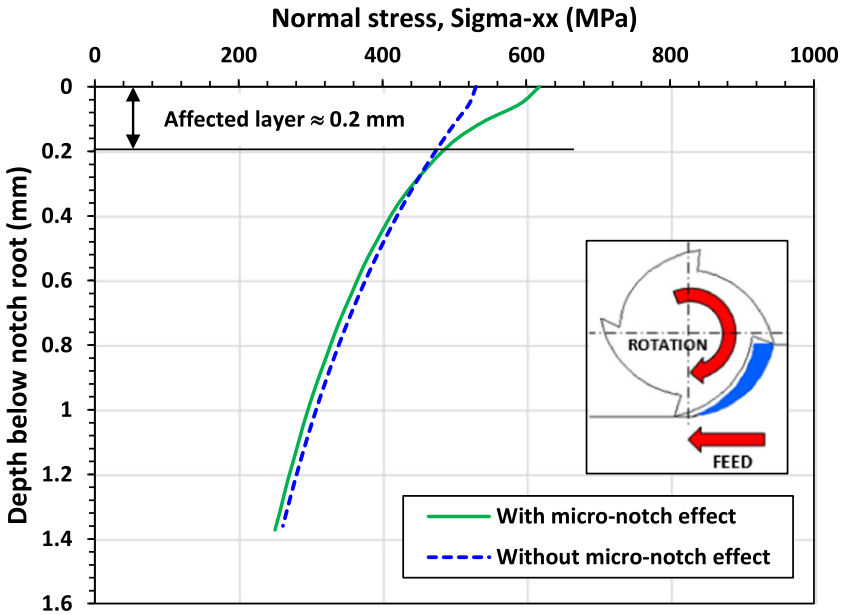

(b)

Fig. 19 The calculated $\sigma_{xx}(z)$ stress profiles with and without micro-notch effect. **a** Case of up-milled surface. **b** Case of down-milled surface

the effect of residual stresses and their evolution under cyclic loading. At endurance limit, the cyclic response at the sample notch root is always characterized by an elastic shakedown behaviour. In this case, the stabilized residual stresses (Eq. 8) can be then superposed to the applied cyclic stresses. Therefore, the total cyclic stress tensor $\sigma_t(t)$ and the total equivalent stress σ_t^{eq} are given by Eqs. 9 and 10, respectively.

$$\underline{\underline{\sigma}}^{*}_{R} = \begin{bmatrix} \sigma^{*}_{Rxx} & 0 & 0 \\ 0 & \sigma^{*}_{Ryy} & 0 \\ 0 & 0 & 0 \end{bmatrix} \tag{8}$$

$$\underline{\underline{\sigma}}_t(t) = \underline{\underline{\sigma}}_{\text{app}}(t) + \underline{\underline{\sigma}}^{*}_{R} = \begin{bmatrix} \sigma^{a}_{xx}\sin(wt) + \sigma^{m}_{xx} + \sigma^{*}_{Rxx} & 0 & 0 \\ 0 & \sigma^{a}_{yy}\sin(wt) + \sigma^{m}_{yy} + \sigma^{*}_{Ryy} & 0 \\ 0 & 0 & 0 \end{bmatrix} \tag{9}$$

$$\sigma_t^{eq} = \tau^{a}_{\text{app}} + \alpha_0\left(P^{\max}_{\text{app}} + P^{*}_{R}\right) \tag{10}$$

where the hydrostatic pressure due to the stabilized residual stresses is expressed by: $P^{*}_{R} = \left(\sigma^{*}_{Rxx} + \sigma^{*}_{Ryy}\right)/3$.

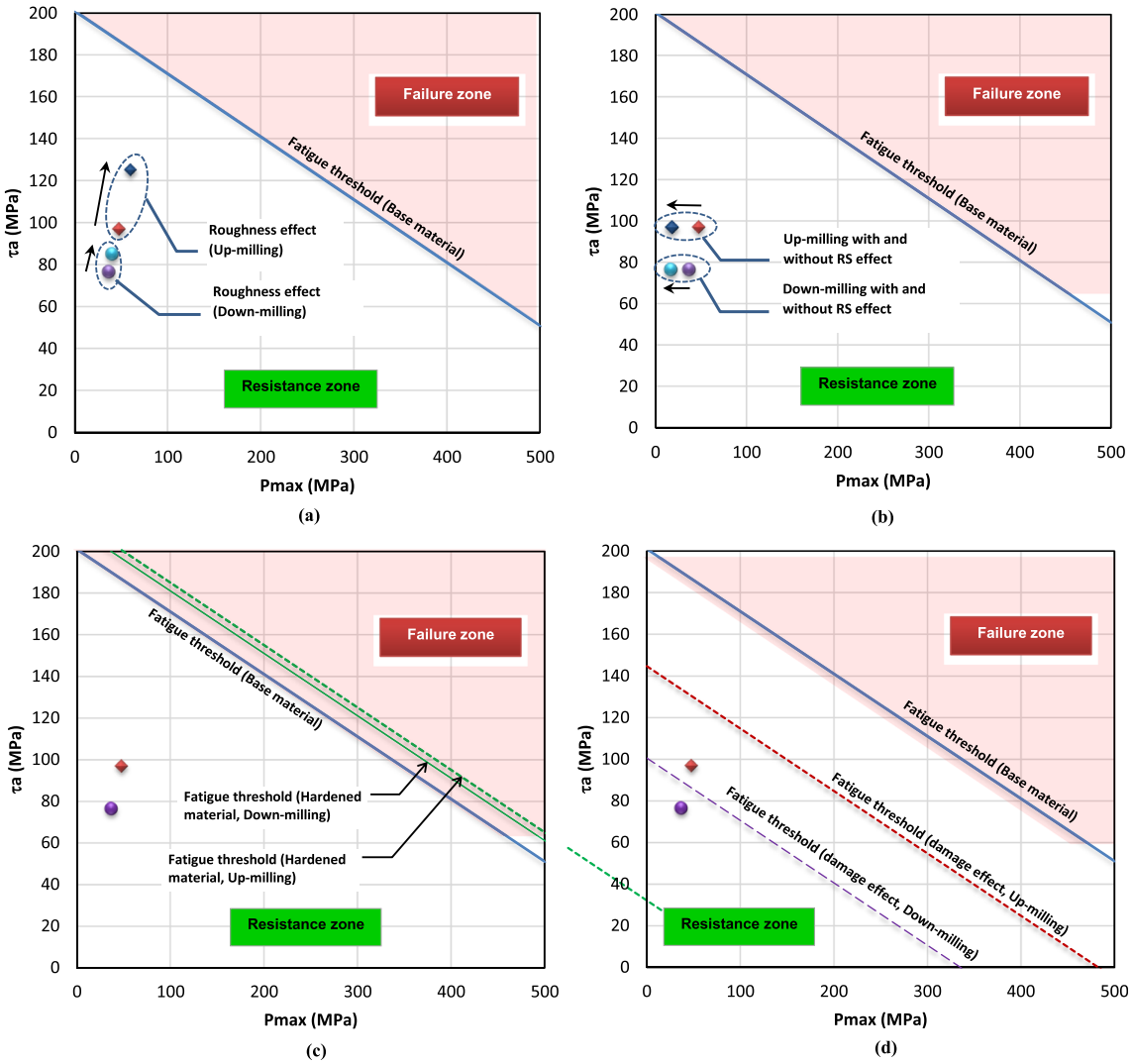

Fig. 20 Dang Van's diagrams showing the surface integrity effects induced by up-milling and down-milling on fatigue strength of X160CrMoV12 steel. **a** Surface roughness effect. **b** Stabilized residual stress effect. **c** Superficial work-hardening effect. **d** Damage effect

The effect of stabilized compressive residual stresses on fatigue strength is estimated by the indicator I_{RS} which is expressed by the difference between the two equivalent stresses σ_{app}^{eq} and σ_t^{eq} with respect to the β_0 constant (Eq. 11). Dang Van's diagram (Fig. 20b) shows that this beneficial effect is traduced by a displacement of the applied loading representative point towards the negative pressures. This effect appears enough significant for the up-milled state ($I_{RS} \approx +14\%$) and lower for the down-milled state ($I_{RS} \approx +7\%$).

$$I_{RS} = \frac{\sigma_{app}^{eq} - \sigma_t^{eq}}{\beta_0} \tag{11}$$

4.4 Prediction of the superficial work-hardening effect

Deperrois [49] proposes to introduce the superficial work-hardening effect in Dang Van's criterion through only the correction of the β_0 base material constant. The α_0 constant is supposed unchanged after surface treatment. In this case, β_0 becomes a variable (β_{hard}) which changes with the local surface density of dislocations. Since the *FWHM* is linked qualitatively to the density of dislocations, then the variable β_{hard} was expressed by a power law of the surface variable $FWHM_S$. A similar relationship was proposed by [50] using the surface micro-hardness HV_S.

$$\beta_{hard} = K(HV_S)^n \tag{12}$$

where K and n are two material coefficients. K is identified using the base material characteristics β_0 and HV_0. The constant n is supposed equals to the monotonic hardening coefficient ($n = 0.119$). This allows to express the β_{hard} constant of the up-milled and down-milled surfaces with the HV_s parameter.

$$\beta_{hard} = \beta_0 \left(\frac{HV_s}{HV_0}\right)^n \tag{13}$$

So, the hardened material constant β_{hard}, whether for up-milled or down-milled surface, is slightly higher than the base material constant ($\beta_0 = 201$ MPa) and equals to 215 MPa and 211 MPa, respectively. This beneficial effect of superficial work-hardening is traduced in Dang Van's criterion by a little increase of the base material resistance domain (Fig. 20c). This effect is estimated by the indicator I_{hard} expressed by the relative difference between the β_{hard} and β_0 constants (Eq. 14), and consequently, it appears more significant for the up-milled surface ($I_{hard} \approx +9\%$) than for the down-milled one ($I_{hard} \approx +5\%$).

$$I_{hard} = \frac{\beta_{hard} - \beta_0}{\beta_0} \tag{14}$$

4.5 Prediction of the damage effect

The shape and the size of the superficial damaging defects induced by up-milling and down-milling operations were characterized by SEM exams at the notch root of specimens. The observed defects such as folds, scales, micro-cracks and micro-cavities are localized at the near-surface layer. These defects can be considered as discontinuities of material at the first affected layer. In the predictive approach of fatigue strength, the damage variable $D(\underline{n})$, proposed by Lemaitre and Chaboche [51], is used to take into account the effect of damage defects. We assume that the first layer representative volume element is damaged homogenously. The superficial damage variable, denoted D_S, is supposed isotropic (independent of direction). The effective cyclic stress tensor taking into account of damage effect is then given by the following relationship:

$$\underline{\underline{\tilde{\sigma}}}(t) = \frac{1}{(1-D_S)}\ \sigma(t) \tag{15}$$

So, the effect of superficial damage results in a reduction of β_0 parameter of Dang Van's criterion by the factor $(1 - D_S)$. The β_{damage} constant of the damaged surface expresses the unfavourable effect of superficial damage on the HCF performance.

$$\beta_{damage} = \beta_0(1-D_S) \tag{16}$$

In this study, the D_S variable is identified by calibration of Dang Van's criterion. The effective equivalent stress σ_{eff}^{eq} is calculated from the effective cyclic stress tensor $\left(\sigma_{eff}(t)\right)$ including the effects of residual stresses and surface roughness and considered equal to the β_0 constant corrected by the work-hardening and damage effects (Eqs. 17 and 18).

$$\underline{\underline{\sigma}}_{eff}(t) = \underline{\underline{\hat{\sigma}}}(t) + \overset{*}{\underline{\underline{\sigma}}}_{RS} \tag{17}$$

$$\sigma_{eff}^{eq} \equiv \hat{\tau}^a + \alpha_0.\left(\hat{P}^{\max} + P_R^*\right) = \beta_0\left(\frac{HV_S}{HV_0}\right)^n (1-D_S) \tag{18}$$

Consequently, the damage variable corresponding to the down-milled surface ($D_S \approx 0.50$) appears higher than that for the up-milled surface ($D_S \approx 0.28$). The superficial damage effect is traduced in Dang Van's diagram (Fig. 20d) by a reducing of resistance domains of down-milled and up-milled surfaces, characterized by β_{damage} equals to 101 MPa and 145 MPa, respectively. The indicator of damage effects (I_{damage}), expressed by the relative difference between the β_{damage} and β_0 constants, was introduced (Eq. 19). This indicator seems to be very higher for the down-milled surface ($I_{damage} \approx -50\%$) than for the up-milled one ($I_{damage} \approx -28\%$).

$$I_{damage} = \frac{\beta_{damge} - \beta_0}{\beta_0} \tag{19}$$

5 Discussion

5.1 Surface integrity

(i) Down-milled surface integrity

In the case of down-milling, the tool teeth attack the surface to be machined at its largest chip thickness, which decreases progressively with the advance of the cutter to cancel at the end of the machining pass. This avoids the burnishing effect and reduces the superficial work-hardening, accordingly. For the thermal effect, the temperature in the contact area between tool and workpiece increases to the maximum while the heat source approaches the machined surface. The transient temperature of the machined surface is relatively high which gives rise to thermal stress [52]. This configuration is generally the best way to machine parts today since it reduces the load from the cutting edge, leaves a better surface finish (chips are removed behind the cutter) and also improves tool life [7].

However, in the case of X160CrMoV12 annealed steel, the superheated scales and chips and not cleared out of the cutting zone are taken up by the ridge of the milling cutter, which deforms them more and presses them against the generated surface to give brittle folds and multiple micro-cracks. These latter are considered as sources of contribution of the additional heat that may explain the distribution of tensile residual stresses associated with this milling mode characterized by relatively lower cutting forces as shown by experimental measurements. The residual stresses induced by down-milling present slight levels which do not exceed 100 MPa in the two surface directions. The induced tensile stresses show that the thermal effect between cutting tool and the workpiece is more important than the mechanical work-hardening effect. The tensile residual stresses are generally generated by the

majority of machining processes such as turning, milling, grinding and drilling due to the presence of the thermal effect in the cutting process [53–57]. The thermal residual stress mechanism can be explained by two successive steps [58]: (i) the heat of cutting process expands the surface layer and produces, in the first step, compressive stresses; (ii) in the second step, the workpiece is then cooled and contractions in the surface layer produce finally tensile residual stresses.

(ii) Up-milled surface integrity

In up-milling, the chip thickness starts at zero and increases towards the end of the cut. The cutting edge has to be forced into the cut, creating higher friction, and consequently, a greater work-hardened surface and tool life decrease (faster tool wear). For the thermal effect, the cooled tool edge indents into the workpiece with the heat source moving away from the machined surface and the transient temperature rising gradually to the maximum. As a result, the thermal effect is minor in the residual stress formation [52]. These thermal and mechanical phenomena are responsible for the poor micro-geometrical state of the machined surface, the strong surface matting and the scratching of hard carbides. These results demonstrate that the friction is characterized by high adhesion between the cutting tool (hard metal) and the machined material (soft material with ferritic matrix at annealed state). The pressure at the surface, created by the intense friction, explains the greater work-hardening on the surface and sub-layers affected by up-milling and their compressive residual stresses. Furthermore, the shear stress resulting from the cutting force induces hard carbide extraction when the tool attacks material.

The creation of compressive residual stresses by the up-milling process can be explained by the predominant mechanical effect in comparison with the thermal effect. Indeed, the contact between teeth of the tool and the workpiece exercises a high pressure on the workpiece and causes plastic stretching of the top layers of the machined surface. Upon unloading, the elastically stressed subsurface layers tend to recover their original dimensions, but the continuity of the material in both zones (the elastic and the plastic) does not allow this to occur. Consequently, a compressive residual stress field (at surface layer) followed by tensile stresses (in sub-layers) is trapped in the treated component. The same mechanism is used by the mechanical surface treatments such as shot-peening, burnishing and rolling that allow to introduce beneficial compressive residual stresses for fatigue strength [59].

5.2 Fatigue behaviour

The fatigue results associated with both up-milling and down-milling modes confirm the important relationship between surface integrity and fatigue strength of machined materials [12–38], expressed by the fatigue limit (σ_e) or the fatigue life (N_{life}). Generally, the surface roughness [14], the damaging superficial defects and the residual stresses [12–15] are the main factors influencing fatigue strength of machined components. Also, the increase of work-hardening tends to improve the resistance to crack initiation on the surface [12]. As explained in the previous section, all these surface integrity parameters are different between the up-milled surface and the down-milled surface. Then, this study attempted to evaluate the surface integrity effects in order to elucidate and discuss the significant degradation of fatigue limit (-21%) of the down-milled surface in comparison with that of the up-milled one. The respective influence of each surface parameter, shown in Fig. 21, was evaluated by using the HCF behaviour predictive approach, based on the multiaxial fatigue criteria. The performance of this approach was validated in the case of shot-peened surfaces [39, 50].

(i) Fatigue behaviour of down-milled surface

For the finished surface by down-milling, the distribution of folds and micro-cracks appears the main surface effect ($\approx -50\%$) that explains the premature damage under cyclic loading in comparison with the surface finished by up-milling. However, the roughness, residual stresses and work-hardening (not exceeding $\approx 9\%$) seem to have less effects on fatigue strength.

The tensile residual stresses become compressive stresses after cyclic relaxation and stabilization at fatigue limit (2×10^6 cycles), and accordingly, play a beneficial effect quite significantly ($\approx +9\%$). This relaxation is due to the accumulation of cyclic plastic strains in the sample notch root of fatigue specimens under cyclic loading [59]. The main residual stress relaxation normally takes place in the first cycle, followed by further gradual relaxation during the life time [60]. The relaxation during the first cycle (quasi-static loading) occurs when the superposition of the applied and residual stresses exceeds the monotonic yield strength of the material in tension and compression, while the relaxation during successive cycles is related to the cyclic yield strength [60, 61]. The latter is the most difficult and has attracted the attention of several researchers by using experimental and numerical approaches [15, 59–64]. In previous work [15], the relaxation of tensile residual stresses has been simulated by a FE model in the case of 316L steel notched specimens finished by grinding and subjected to 3-point bending ($R_\sigma = 0.1$). It was found that the cyclic behaviour of the notch root is characterized by a gradual plastic shakedown with hysteresis loops. During the shakedown process, both cyclic ratcheting and mean stress relaxation occur simultaneously with decrease rate. This process tends after a great number of cycles to an elastic-shakedown response with closed loop (i.e., no further plastic deformation). Therefore, the grinding residual stresses reach a stabilized state.

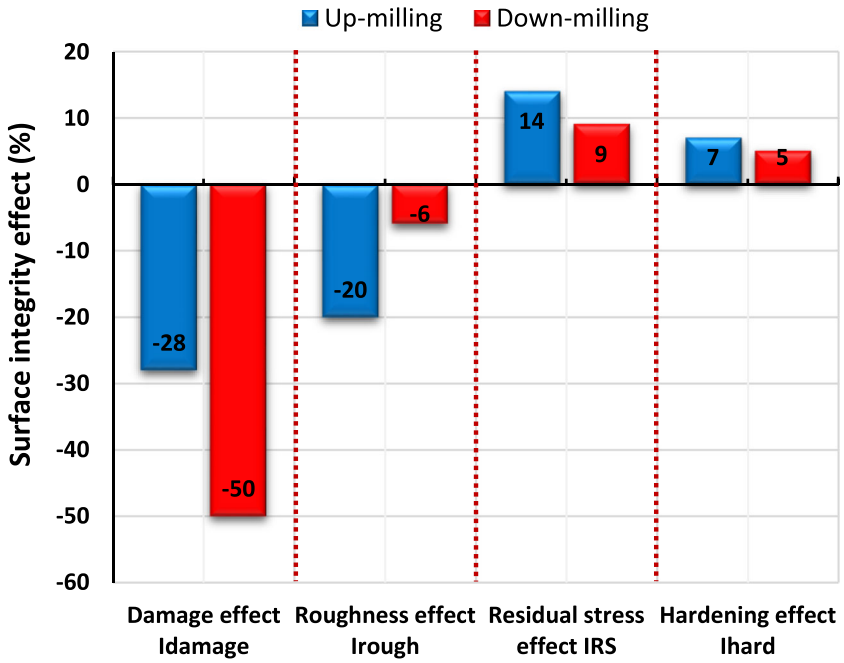

Fig. 21 Comparison of surface integrity effects of up-milling and down-milling operations on fatigue strength of X160CrMoV12 steel

The surface roughness is characterized by a significant level of the maximum roughness depth ($R_{max} = 28$ µm), but its detrimental effect in fatigue limit seems to be relatively low (≈ − 6%). This prediction is in good agreement with the experimental results developed by Taylor and Clancy [43]. They revealed in the case of stress relieved AISI 4140 steel that a coarse milling operation ($Ra = 1.1$–1.8 µm and $R_{max} = 26$–34 µm) reduces the fatigue limit of ≈ − 5% in comparison with the polishing operation ($Ra = 0.1$–0.3 µm and $R_{max} = 3$–5 µm).

The work-hardening is relatively low ($HV_s/HV_0 \approx 145\%$) and affects a very superficial layer of ≈ 50 µm. This effect appears relatively slight beneficial for fatigue strength (≈ + 5%). This is in good agreement with many works showing that the work-hardening effect is generally lower than the residual stress effect [13, 14, 39].

(ii) Fatigue behaviour of up-milled surface

The up-milled surface is characterized by a density of micro-cavities, and according to predictive calculation, these defects seem to be less detrimental (≈ − 28%) than the damaging defects (folds and micro-cracks) induced by down-milling (− 50%). This justifies the better fatigue strength of up-milled surface in comparison with the down-milled one, in spite of its poor micro-geometric quality [16, 18]. Indeed, the roughness effect induced by up-milling (≈ − 20%) appears largely higher in comparison with that in the down-milled surface (≈ − 6%), because the levels of micro-geometrical ($Ra = 11$ µm; $R_{max} = 87$ µm) are enough significant in fatigue strength [12]. Nerveless, this detrimental micro-geometrical effect is nearly compensated by the combined beneficial effects of work-hardening (≈ + 7%) and stabilized compressive residual stresses (≈ + 14%).

The compressive residual stresses induced by up-milling are produced by mechanic plastic stretching of the near-surface layers when the tooth of the tool attacks tangentially the material. These stresses are beneficial for fatigue strength like those induced by the mechanical surface treatments such as shot-peening, burnishing and rolling [59]. However, their effect is reduced by relaxation at fatigue limit. The relaxation of compressive residual stresses in notched specimens under two bending tests ($R_\sigma = 0$ and $R_\sigma = \infty$) has been studied by Peiffer [59] using the XRD method [60]. The author observed that, with $R_\sigma = 0$, significant relaxation during the first cycles was followed by stabilization. This observation proves with the partial relaxation of residual stresses in the up-milled surface layer. In contract, with $R_\sigma = \infty$, it was noted significant but progressive relaxation.

The work-hardening is higher ($HV_s/HV_0 \approx 175\%$) in the up-milled surface and affects an important superficial layer of ≈ 300 µm. However, this micro-structural effect is estimated slightly increases (≈ + 7%) in comparison with the down-milling mode (≈ + 5%). This proves that the superficial work-hardening does not affect significantly the fatigue strength for the annealed X160CrMoV12 steel.

6 Conclusion

The influences of both up-milling and down-milling on surface integrity and fatigue strength of X160CrMoV12 steel have been investigated experimentally and evaluated by using a predictive approach based on Dang Van's multiaxial fatigue

criterion. The principal findings of this study are summarized as follows:

(i) The down-milling operation induces a poor surface integrity characterized by a severe damage defects (metal folds and micro-cracks) and slightly affected by residual tensile stresses, roughness and surface hardening. The fatigue limit of this down-milled surface is lower of about − 21% in comparison with that of the up-milled surface. This degradation is explained by the damage effect, which is estimated to affect greatly the fatigue limit of the base material by about − 50%, while the other effects are relatively lower.

(ii) The up-milling operation induces a surface integrity which appears to be better than the down-milled surface integrity towards fatigue performance. This machined surface is highly work-hardened and subjected to compressive residual stresses, but it includes a density of micro-cavities and characterized by higher surface roughness. The damaging defects of this surface are less detrimental to fatigue limit of the base material (≈ − 28%) than those induced by down-milling. The detrimental roughness effect seems to be relatively higher (≈ − 20%), but it is greatly reduced by the beneficial effects of work-hardening (≈ + 7%) and compressive residual stresses (≈ + 14%).

(iii) The experimental and predictive evaluations show obviously the advantage of up-milling that allows a better control of surface damaging defect and, consequently, improves the fatigue strength of the X160CrMoV12 in comparison with the down-milling configuration.

References

1. Walsh RA, Cormier DR (2016) McGraw-Hill Machining and metalworking handbook, 3rd ed.
2. San-Juan M, Martin O, de Tiedra M d P, Santos FJ, Lopez R, Cebrian JA (2015) Study of cutting forces and temperatures in milling of AISI 316L. Procedia Engineering 132:500–506. https://doi.org/10.1016/j.proeng.2015.12.525
3. Toh CK (2005) Comparison of chip surface temperature between up and down milling orientations in high speed rough milling of hardened steel. J Mater Process Technol 167:110–118. https://doi.org/10.1016/j.jmatprotec.2004.10.004
4. Beizhi L, Yingzi Y, Jianguo Y (2015) Influence and optimization criterion of milling modes and process parameters on residual stress. ICADME, pp 1874–1879
5. Scholtes B (1987) Residual stresses introduced by machining. In: Niku-Lari A (ed) Advances in surface treatments, vol 4. Pergamon Press, Oxford, pp 59–71
6. Caixu Y, Haining G, Xianli L, Steven YL (2018) Part functionality alterations induced by changes of surface integrity in metal milling process: a review. Appl Sci 8(12):2550. https://doi.org/10.3390/app8122550
7. Hadi MA, Ghani JA, Che Haron CH, Kasim MS (2013) Comparison between up-milling and down-milling operations on tool wear in milling Inconel 718. Procedia Eng 68:647–653. https://doi.org/10.1016/j.proeng.2013.12.234
8. Bouzakis KD, Makrimallakis S, Katirtzoglou G, Bouzakis E, Skordaris G, Maliaris G, Gerardis S (2012) Coated tools' wear description in down and up milling based on the cutting edge entry impact duration. CIRP Ann Manuf Technol 61:115–118 https://doi.org/10.1016/j.cirp.2012.03.040
9. Bouzakis KD, Makrimallakis S, Skordaris G, Bouzakis E, Kombogiannis S, Katirtzoglou G, Maliaris G (2014) Coated tools' performance in up and down milling stainless steel, explained by film mechanical and fatigue properties. Proceedings of the 11th international conference "THE-A" coatings in manufacturing engineering 97-116
10. Insperger T, Mann BP, Stepan G, Bayly PV (2003) Stability of up-milling and down-milling, part 1: alternative analytical methods. Int J Mach Tool Manu 43:25–34. https://doi.org/10.1016/S0890-6955(02)00159-1
11. Michalik P, Zajac J, Hatala M, Mital D, Fecova V (2014) Monitoring surface roughness of thin-walled components from steel C45 machining down and up milling. Measurement 58:416–428. https://doi.org/10.1016/j.measurement.2014.09.008
12. Sahara H (2005) The effect on fatigue life of residual stress and surface hardening resulting from different cutting conditions of 0.45%C steel. Int J Mach Tools Manuf 45:131–136. https://doi.org/10.1016/j.ijmachtools.2004.08.002
13. Gao Y, Li X, Yang Q, Yao M (2007) Influence of surface integrity on fatigue strength of 40CrNi2Si2MoVA steel. Mater Lett 61(2):466–469. https://doi.org/10.1016/j.matlet.2006.04.089
14. Novovic D, Dewes RC, Aspinwall DK, Voice W, Bowen P (2004) The effect of machined topography and integrity on fatigue life. Int J Mach Tools Manuf 44:125–134. https://doi.org/10.1016/j.ijmachtools.2003.10.018
15. Laamouri A, Sidhom H, Braham C (2013) Evaluation of residual stress relaxation and its effect on fatigue strength of AISI 316L stainless steel ground surfaces: experimental and numerical approaches. Int J Fatigue 48:109–121. https://doi.org/10.1016/j.ijfatigue.2012.10.008
16. Javidi A, Rieger U, Eichlseder W (2008) The effect of machining on the surface integrity and fatigue life. Int J Fatigue 30:2050–2055. https://doi.org/10.1016/j.ijfatigue.2008.01.005
17. Pramanik A, Dixit AR, Chattopadhyaya S, Uddin MS, Dong Y, Basak AK, Littlefair G (2017) Fatigue life of machined components. Adv Manuf 5(1):59–76. https://doi.org/10.1007/s40436-016-0168-z
18. Geng GS, Xu JH (2008) Surface integrity and fatigue property of a high speed milled titanium alloy. Adv Mater Res 53-54:305–310. https://doi.org/10.4028/www.scientific.net/AMR.53-54.305
19. Bentley SA, Mantle AL, Aspinwall DK (1999) The effect of machining on the fatigue strength of a gamma titanium aluminide intermetallic alloy. Intermetallics 7:967–969. https://doi.org/10.1016/S0966-9795(99)00008-4
20. Moussaoui K, Mousseigne M, Senatore J, Chieragatti R, Lamesle P (2015) Influence of milling on the fatigue lifetime of a Ti6Al4V titanium alloy. Metals 5:1148–1162. https://doi.org/10.3390/met5031148
21. Guoliang L, Ghuanzhen H, Hangtao Z, Zhanqiang L, Yue L (2017) The modified surface properties and fatigue life of Incoloy A286 face-milled at different cutting parameters. Mater Sci Eng A704:1–9. https://doi.org/10.1016/j.msea.2017.07.072
22. Li X, Guan C, Zhao P (2018) Influences of milling and grinding on machined surface roughness and fatigue behavior of GH4169 superalloy workpieces. Chin J Aeronaut 31(6):1399–1405. https://doi.org/10.1016/j.cja.2017.07.013

23. Ojolo SJ, Orisaleye IJ, Obiajulu N (2014) Machining variables influence on the fatigue life of end-milling aluminum alloy. Int J Mater Sci Appl 3(6):391–398 http://www.sciencepublishinggroup.com/j/ijmsa
24. Piska M, Ohnistova P, Hornikova J, Hervoches C A Study of progressive milling technology on surface topography and fatigue properties of the high strength aluminum alloy 7475-T7351. Proceedings of the 17th International Conference on New Trends in Fatigue and Fracture. https://doi.org/10.1007/978-3-319-70365-7_2
25. Yao C, Wu D, Jin Q, Huang X, Ren J, Zhang D (2013) Influence of high-speed milling parameter on 3D surface topography and fatigue behavior of TB6 titanium alloy. Trans Nonferrous Met Soc China 23:650–660. https://doi.org/10.1016/S1003-6326(13)62512-1
26. Ghanem F, Ben Fredj N, Sidhom H, Braham C (2011) Effects of finishing processes on the fatigue life improvements of electro-machined surfaces of tool steel. Int J Adv Manuf Technol 52(5–8):583–595. https://doi.org/10.1007/s00170-010-2751-y
27. McClung RC (2007) A literature survey on the stability and significance of residual stresses during fatigue. Fatigue Fract Eng Struct 30(3):173–205. https://doi.org/10.1111/j.1460-2695.2007.01102.x
28. Yao CF, Tan L, Ren JX, Lin Q, Liang YS (2014) Surface integrity and fatigue behavior for high-speed milling Ti–10V–2Fe–3Al titanium alloy. J Fail Anal Prev 14:102–112. https://doi.org/10.1007/s11668-013-9772-4
29. Moussaoui K, Mousseigne M, Senatore J, Chieragatti R (2015) The effect of roughness and residual stresses on fatigue life time of an alloy of titanium. Int J Adv Manuf Technol 78:557–563. https://doi.org/10.1007/s00170-014-6596-7
30. Huang W, Zhao J, Xing A, Wang G, Tao H (2018) Influence of tool path strategies on fatigue performance of high-speed ball-end-milled AISI H13 steel. Int J Adv Manuf Technol 94:371–380. https://doi.org/10.1007/s00170-017-0841-9
31. Yang D, Zhanqiang L (2017) Surface integrity generated with peripheral milling and the effect on low-cycle fatigue performance of aeronautic titanium alloy Ti-6Al-4V. Aeronautical J, New Series 122(1248):1–17. https://doi.org/10.1017/aer.2017.136
32. Arola D, Ramulu M (1999) An examination of the effects from surface texture on the strength of fiber-reinforced plastics. J Compos Mater 33(2):102–123. https://doi.org/10.1177/002199839903300201
33. Arola D, Williams CL (2002) Estimating the fatigue stress concentration factor of machined surfaces. Int J Fatigue 24(9):923–930. https://doi.org/10.1016/S0142-1123(02)00012-9
34. Wang X, Huang C, Zou B, Liu G, Zhu H, Wang J (2018) Experimental study of surface integrity and fatigue life in the face milling of Inconel 718. Front Mech Eng 13(2):243–250. https://doi.org/10.1007/s11465-018-0479-9
35. Yao CF, Wu DX, Jin QC, Huang XC, Ren JX, Zhang DH (2013) Influence of high-speed milling parameter on 3D surface topography and fatigue behavior of TB6 titanium alloy. Trans Nonferrous Met Soc China 23:650–660. https://doi.org/10.1016/S1003-6326(13)62512-1
36. Novovic D, Aspinwall DK, Dewes RC, Bowen P, Griffiths B (2016) The effect of surface and subsurface condition on the fatigue life of Ti–25V–15Cr–2Al–0.2C %wt alloy. CIRP Ann Manuf Technol 65(1):523–528. https://doi.org/10.1016/j.cirp.2016.04.074
37. Liu G, Huang C, Zhu H, Liu Z, Liu Y, Li C (2017) The modified surface properties and fatigue life of Incoloy A286 face-milled at different cutting parameters. Mater Sci Eng A 704:1–9. https://doi.org/10.1016/j.msea.2017.07.072
38. Yang D, Liu Z, Xiao X, Xie F (2018) The effects of machining-induced surface topography on fatigue performance of titanium alloy Ti-6Al-4V. Procedia CIRP 71:27–30. https://doi.org/10.1016/j.procir.2018.05.015
39. Fathallah R, Laamouri A, Sidhom H, Braham C (2014) High cycle fatigue behavior prediction of shot peened parts. Int J Fatigue 26(10):1053–1067. https://doi.org/10.1016/j.ijfatigue.2004.03.007
40. Dang Van K (1999) Introduction to fatigue analysis in mechanical design by the multiscale approach, in : K. Dang Van, I.V. Papadoupoulos, High Cycle Metal Fatigue in the Context of Mechanical Design. CISM Courses and Lectures N° 392, Springer-Verlag, pp 57–88
41. ISO 25178-22012 (2017) Geometrical product specifications (GPS) - surface texture: areal – Part 2: terms, definitions and surface texture parameters. Ed. International Organization for Standardization (ISO)
42. Hertzberg RW (1996) Deformation and fracture mechanics of engineering materials. John Wiley & Sons, Inc
43. Taylor D, Clancy OM (1991) Fatigue performance of machined surfaces. Fatigue Fract Eng Mater Struct 14(2–3):329–336. https://doi.org/10.1111/j.1460-2695.1991.tb00662.x
44. Ås SK, Skallerud B, Tveiten BW, Holme B (2005) Fatigue life prediction of machined components using finite element analysis of surface topography. Int J Fatigue 27:1590–1596. https://doi.org/10.1016/j.ijfatigue.2005.07.031
45. Ås SK, Skallerud B, Tveiten BW (2008) Surface roughness characterization for fatigue life predictions using finite element analysis. Int J Fatigue 30:2200–2209. https://doi.org/10.1016/j.ijfatigue.2008.05.020
46. Hibbitt, Karlsson, Sorenson, & Inc. (2014) ABAQUS standard user's manual, version 6.14, USA
47. Peterson RE (1974) Stress concentration factors. John Wiley and Sons, New York
48. Mitchell MR (1979) A unified predictive technique for the fatigue resistance of cast ferrous-based metals and high hardness wrought steels, SAE/SP-79/448, Soc. of automotive Engrs
49. Deperrois A, Castex L, Dang Van K, Merrien P, Bignonnet A (1990) High cycle fatigue life of surface hardened steels under multi-axial loading, in: H. Kitagawa, T. Tanaka (Eds.). Proceedings of the fourth international fatigue conference, vol. 4, Hawaii, USA, July 15-20, pp 2417-22
50. Sidhom N, Laamouri A, Fathallah R, Braham C, Lieurade HP (2005) Fatigue strength improvement of 5083 H11 Al-alloy T-welded joints by shot peening : experimental characterization and predictive approach. Int J Fatigue 27(7):729–747. https://doi.org/10.1016/j.ijfatigue.2005.02.001
51. Lemaitre J (1985) A continuous damage mechanics model for ductile fracture. J Eng Mater Technol 107:83–89
52. Huanga X, Zhanga X, Dinga H (2017) An enhanced analytical model of residual stress for peripheral milling. Procedia CIRP 58:387–392. https://doi.org/10.1016/j.procir.2017.03.245
53. García Navas V, Ferreres I, Marañón JA, Garcia-Rosales C, Gil Sevillano J (2008) Electro-discharge machining (EDM) versus hard turning and grinding-comparison of residual stresses and surface integrity generated in AISI O1 tool steel. J Mater Process Technol 195(1–3):186–194. https://doi.org/10.1016/j.jmatprotec.2007.04.131
54. Outeiro JC, Pina JC, M'Saoubi R, Pusavec F, Jawahir IS (2008) Analysis of residual stresses induced by dry turning of difficult-to-machine materials. CIRP Ann Manuf Technol 57:77–80. https://doi.org/10.1016/j.cirp.2008.03.076
55. Ee KC, Dillon OW Jr, Jawahir IS (2005) Finite element modeling of residual stresses in machining induced by cutting using a tool with finite edge radius. Int J Mech Sci 47:1611–1628. https://doi.org/10.1016/j.ijmecsci.2005.06.001
56. Hua Y, Liu Z (2018) Experimental investigation of principal residual stress and fatigue performance for turned nickel-based superalloy Inconel 718. Materials 11:879. https://doi.org/10.3390/ma11060879

57. Liang SY, Su JC (2007) Residual stress modeling in orthogonal machining. Annals of the CIRP Vol. 56/1/2007. https://doi.org/10.1016/j.cirp.2007.05.018
58. Gunnberg F, Escursell M, Jacobson M (2006) The influence of cutting parameters on residual stresses and surface topography during hard turning of 18MnCr5 case carburised steel. J Mater Process Technol 174(1–3):82–90. https://doi.org/10.1016/j.jmatprotec.2005.02.262
59. Schulze V (2006) Modern mechanical surface treatment: states, stability, effects. WILEY-VCH Verlag GmbH & Co. KGaA, Weinheim
60. Kodama S (1972) The behaviour of residual stress during fatigue stress cycles In: Proceedings of the international conference on mechanical behaviour of materials II, society of material science, Kyoto, Japan, pp 111–18
61. Dalaei K, Karlsson B, Svensson LE (2011) Stability of shot peening induced residual stresses and their influence on fatigue lifetime. Mater Sci Eng A528:1008–1015. https://doi.org/10.1016/j.msea.2010.09.050
62. Zhuang WZ, Halford GR (2001) Investigation of residual stress relaxation under cyclic load. Int J Fatigue 23:31–37. https://doi.org/10.1016/S0142-1123(01)00132-3
63. Smith DJ, Farrahi GH, Zhu WX, McMahon CA (2001) Experimental measurement and finite element simulation of the interaction between residual stresses and mechanical loading. Int J Fatigue 23:293–302. https://doi.org/10.1016/S0142-1123(00)00104-3
64. Gong K, Milley A, Lu J (2001) Design tool on fatigue for 3D components with consideration of residual stresses. SAE 2001 world congress, fatigue research & applications (Part A&B), Detroit, MI, USA, pp 1-6